Multimedia Tools and Applications (2020) 79:17793–17815
https://doi.org/10.1007/s11042-020-08696-x

Evaluation of driver drowsiness using respiration analysis by thermal imaging on a driving simulator

Serajeddin Ebrahimian Hadi Kiashari[1] · Ali Nahvi[1] · Hamidreza Bakhoda[1] · Amirhossein Homayounfard[1] · Masoumeh Tashakori[1]

Received: 8 May 2019 / Revised: 28 November 2019 / Accepted: 28 January 2020 /
Published online: 21 February 2020

Abstract
In this paper, a new non-intrusive driver drowsiness detection method is introduced based on respiration analysis using facial thermal imaging. Drowsiness is the cause of many driving accidents all over the world. Drivers' respiration system undergoes significant changes from wakefulness to drowsiness and can be used to detect drowsiness. Current respiration measurement methods are intrusive and uncomfortable making respiration the least measured vital sign during driving. In this paper, a new method is presented based on facial thermal imaging to analyze drivers' respiration signal non-intrusively. Thirty subjects are tested in a car simulator. They are fully awake at the beginning and experience drowsiness during the tests. The mean and the standard deviation of the respiration rate and the inspiration-to-expiration time ratio are extracted from the subjects' respiration signal. To detect drowsiness, the Support Vector Machine (SVM) and the K-Nearest Neighbor (KNN) classifiers are used. The Observer Rating of Drowsiness method is used for scoring the drowsiness level and validating the proposed method. The performance and the results of both methods are presented and compared. The results indicate that drowsiness can be detected with the accuracy of 90%, sensitivity of 92%, specificity of 85%, and precision of 91%.

Keywords Drowsiness detection · Thermal imaging · Non-contact monitoring · Respiration rate · Driver monitoring system · Driving simulator

1 Introduction

Over the last decade, driver drowsiness detection systems have attracted the attention of many researchers to prevent car crashes. In every road accident, road, vehicle and driver play important roles. Human error is regarded as the most important factor in road

✉ Serajeddin Ebrahimian Hadi Kiashari
sebrahimian@mail.kntu.ac.ir

[1] Faculty of Mechanical Engineering, K.N. Toosi University of Technology, Tehran, Iran

accidents at the present time [53]. In recent years, several papers [3, 19, 34, 45, 48, 50] have presented in-vehicle drowsiness detection systems to compensate for the drawbacks of the out-of-vehicle systems.

Driver drowsiness detection systems are divided into three broad categories based on physiological signals, the driver's facial characteristics and vehicle dynamics [49]. Systems using physiological signals are very accurate in determining the driver's status. However, most physiological sensors interfere with controlling the car, which makes them impossible to be used in real situations due to their intrusive nature [49]. In addition, the use of systems based on the vehicle dynamics data is accompanied by various challenges and a weak performance is expected due to the impact of environmental factors such as road geometry, traffic, vehicle characteristics and low processing speed [49]. The use of driver's facial images and extraction of data from the driver's blinking, movement, turning of the head and yawning shows acceptable results in a controlled laboratory. However, the performance of such systems drops significantly in real situations due to non-ideal conditions such as unpredictable changes in the environment [49].

The high accuracy of physiological-based drowsiness detection systems makes them more reliable compared to other drowsiness detection methods [49]. Physiological signals such as electroencephalography (EEG), electrooculography (EOG), electrocardiography (ECG), and electromyography (EMG) signals are frequently used in drowsiness detection applications and show very high detection rates [4, 9, 36, 41, 52]. Due to the intrusive nature of physiological sensors, most physiological drowsiness detection systems cannot be used while driving. In some studies, physiological methods have been used as a reference method to validate the performance of proposed systems [12, 15]. Due to high accuracy of physiological based drowsiness detection methods, a non-contact and non-intrusive physiological data acquisition can lead to an accurate method in real situations.

Respiration system undergoes significant changes from wakefulness to sleep. Respiration states vary based on physiological conditions. However, respiration is the least measured vital sign due to the uncomfortable nature of traditional respiration monitoring methods. Respiration features vary significantly from wakefulness to sleep [16, 57]. Reduction in muscular tone and metabolic rate, and alteration of chemical/non-chemical responses affect breathing in sleep [64]. Changes such as increase in upper airways impedance, reduction in minute ventilation and attenuation in ventilatory response to CO2 occur from wakefulness to sleep [64].

In recent years, several non-intrusive respiration-monitoring methods have been introduced based on different types of imaging [5, 6, 39, 54]. Some studies measure respiration through visual imaging techniques by measuring chest and abdomen movements [5, 6, 54]. Light variations especially at night reduce the performance of these methods. Thermal imaging has shown promising results in monitoring the respiration of drivers. Murthy et al. [39] monitored respiration using thermal imaging techniques based on temperature variations of the region under the nose in every inspiration and expiration of wakeful subjects.

Thermal infrared imaging has been used in a vast variety of applications in the past decade [22]. Thermal imaging is a passive process, which means it only works using the natural radiation emitted by the body without any direct contact or applying external radiation [22]. In some studies, thermal imaging was used to monitor human vital signs such as forehead blood flow, carotid pulse, and respiration signal [17, 23, 66]. Thermal imaging is used in several studies for monitoring respiration and is highly correlated with traditional respiration measurement methods [7, 32, 40]. The non-contact nature of thermal imaging and its ability to extract vital signs make it a suitable choice for drowsiness detection.

In this paper, thermal imaging is used to monitor the respiration of drowsy drivers. The respiration rate and inspiration-to-expiration time ratio are extracted from the respiration signal. The mean and standard deviation of the extracted features are used to detect drivers' drowsiness status in 2-min intervals using support vector machine (SVM) and K-nearest Neighbors (KNN) classification methods. The results of the classification methods are compared based on different features. The output of the system is validated using Observer Rating of Drowsiness (ORD) method. The experiments are conducted on 30 subjects to evaluate the proposed drowsiness detection system. In section 2, the details of the test protocols are described along with the feature extraction method. Section 3 presents the experimental results. The assumptions and the scope of validity of the results are presented in section 4. The paper is concluded in section 5.

2 Materials and methods

2.1 Signal acquisition

Signal acquisition is the most important part of any physiological drowsiness detection system. The intrusive nature of most physiological measurement systems makes them unusable in actual driving conditions. Temperature changes caused by inspiration and expiration in the region under the nose and nostrils (respiration regions) can be detected by thermal imaging. Several studies have been conducted on the use of thermal imaging as a respiration measurement method [2, 17, 42]. These methods use physiological or geometrical features of a face in order to detect the respiration region and then use a target tracker to track the region in the upcoming frames. None of the previous studies are specifically conducted for driving conditions. Physiological features of the face, such as its hottest and the coldest regions, can change as a result of the physiological or the mental state of the person. Geometrical features of the face can also be altered by the movement and the tilt of the driver's head. Thus, an accurate and robust method is needed for respiration measurement during driving.

In this paper, a robust and automated method is proposed to detect the respiration region of the face in thermal videos. First, the temporal variations of the first few seconds of the thermal image sequence is used to locate the respiration region. The human normal respiration rate varies between 12 and 20 breaths per minute [62]. Therefore, the maximum possible time interval between two consecutive breaths is about 5 s. The regions of the images with a high variation in the first five seconds of the thermal image sequence are located as possible respiration region candidates. The difference between the two consecutive frames of I_n and I_{n-1} is represented by s_n for each pixel coordinates of (x, y) as follows:

$$s_n(x,y) = I_n(x,y) - I_{n-1}(x,y) \tag{1}$$

Small temporal changes are eliminated by discarding temporal changes that are less than half of the maximum norm of the $s_n(x, y)$ as follows:

$$s_n^*(x,y) = \begin{cases} s_n(x,y) & \text{if } s_n(x,y) > \|s_n\|_\infty \\ 0 & \text{otherwise} \end{cases} \tag{2}$$

The sum of the differences of the successive frames *SD* is calculated for the last 5 s as follows:

$$SD = \sum_{n=1}^{5F_s} {s_n}^*(x,y) \tag{3}$$

where F_s is the sampling rate of the thermal camera.

Figure 1(a) shows a typical frame of the thermal video. Figure 1(b) shows the SD image matrix for the next 5 s after that frame. Figure 1(b) shows the respiration region, the eyes, and the head contour exhibit high temporal changes after a 5-s time interval.

The respiration region exhibits big temporal changes and needs to be separated from other regions. First, in order to distinguish the head contour from other regions, we apply the Canny edge detector [27] and then dilate the edges as shown in Fig. 2(a). The head contour is separated from other regions by removing small-edge objects as shown in Fig. 2(b). The localized head contour is shown in Fig. 2(c). By removing the head contour, three major regions including the left eye, the right eye, and the respiration region are distinguished from other regions by applying a thresholding method as follows:

$$B(x,y) = \begin{cases} 1 & if\ R(x,y) > \dfrac{\max_{w*w} R(x,y)}{2} \wedge R(x,y) > t \\ 0 & otherwise \end{cases} \tag{4}$$

where $B(x, y)$ is the binary image that includes only the eyes and the respiration region, $R(x, y)$ is the *SD* image after removing the head contour, $\max_{w*w} R(x, y)$ is the maximum pixel intensity of R in the $w * w$ neighborhood centered at (x, y), and t is a threshold parameter set to 90 to reduce the probability of the presence of small regions in the final image. The size of the neighbor w is set to 5. Figure 2(d) shows eyes and respiration region after applying this thresholding method.

The respiration region is located at the lowest position among the three regions as shown in Fig. 2(d). This fact never changes except when there is a head tilt of more than about 45 degrees relative to the human sagittal plane, which would rarely last for more than 5 s. Therefore, the respiration region can be separated from other regions robustly.

After locating the respiration region, a tracker is applied to track the region on the upcoming frames. Several tracking algorithms have been presented for target tracking in visible images [43]. Several studies have used visible image tracking algorithms in thermal images [18, 42]. The spatio-temporal context learning method is used in the present study. This method is based on modeling the statistical correlation of the low-level characteristics of an image, such as color intensity and the location of the tracking region and the surrounding region, through extracting a spatio-temporal

(a) (b)

Fig. 1 (a) A typical frame of the thermal video; (b) variations of the thermal image sequence for the next 5 s

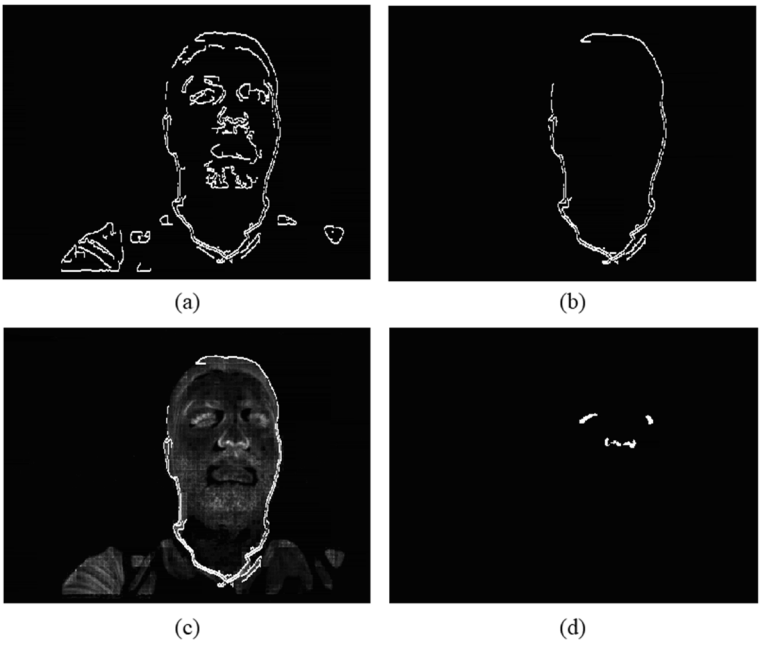

Fig. 2 Demonstration of the process of respiration region localization: (a) dilated edges of the sum of the differences of the successive frames; (b) edges of the sum of the differences of the successive frames after removing small edges objects; (c) head contour localization; (d) localization of the eyes and the respiration region by applying the proposed thresholding method

relationship between the targets and the surrounding regions based on Bayesian structure [65]. In this method, the tracking takes place using a confidence map, which represents an estimate of the probable location of the region and maximizes the value of the region [65].

$$x^*_{t+1} = \arg\max c_{t+1}(x) \tag{5}$$

where x^*_{t+1} is the center of the target region in the next frame $t+1$ and $c_{t+1}(x)$ represents the probable presence of the target region and is calculated as follows [65]:

$$c_{t+1}(x) = F^{-1}\left(F\left(H^{stc}_{t+1}(x)\right) \odot F\left(I_{t+1}(x)\omega_{\sigma t}\left(x - x^*_t\right)\right)\right) \tag{6}$$

where F represents the Fourier transform,$\odot$ is the inner product, H^{stc}_{t+1} represents the model of the spatio-temporal context, $I(.)$ is the image intensity and $\omega_{\sigma t}$is the confident map.

Figure 3 shows the overall performance of the tracking algorithm method in a drowsiness detection test.

The respiration region is localized in the first few seconds of the thermal video in Fig. 3(a) and is then tracked in the following frames despite head movements as shown in Fig. 3 (b), (c), (d), (e) and (f). This method uses thermal variations at the first 5 s of the thermal video to localize the respiration region. The driver's head should not move quickly in this first 5-s interval to make an accurate localization possible.

Finally, the respiration signal is formed by putting together the mean of the respiration region pixels in every frame. The respiration signal is shown in Fig. 4 for one subject. Figure 4(a) shows the respiration signal during a drowsiness test. The large peaks in the respiration signal are due to the movements of the driver's head. Figure 4(b) shows a 1-min

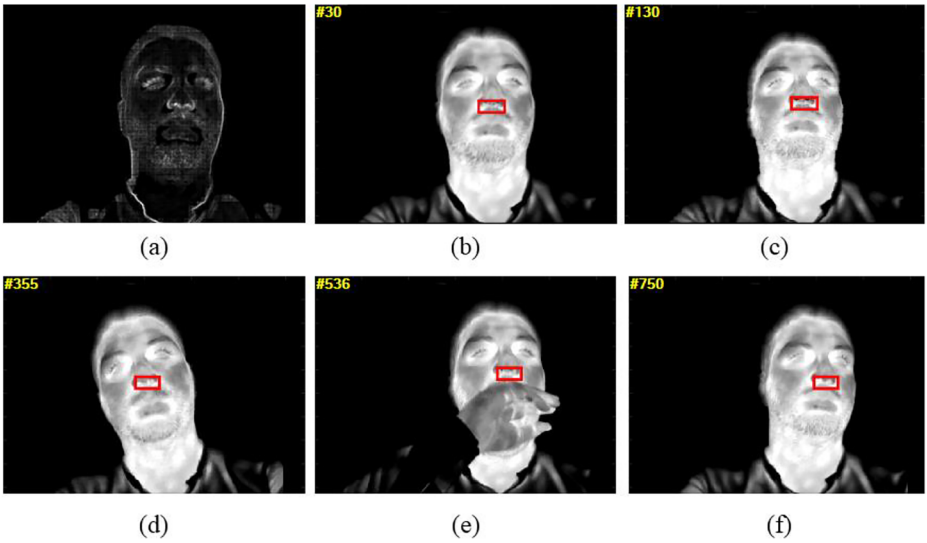

Fig. 3 Region tracking algorithm performance in different frames

epoch of the respiration signal. In order to eliminate high-frequency noises, a fourth-order Butterworth low-pass filter with a cut-off frequency of 0.6 Hz is used.

2.2 Feature extraction

Several features of the respiration system alter from wakefulness to sleep. The most noticeable changes in the respiration signal are changes in the respiration rhythm. Previous studies showed noticeable changes in the respiration rate during transition from wakefulness to drowsiness [32, 47,

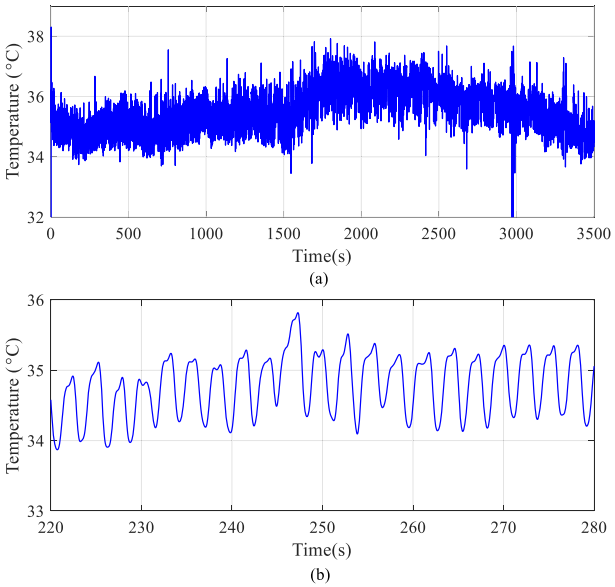

Fig. 4 (a) Respiration signal during a drowsiness test; (b) during a 1-min epoch of the test

60]. The variations of the inspiration time and the expiration time have been studied in different stages of sleep, but not in drowsiness stages so far [16, 57]. In this paper, the respiration rate and the inspiration-to-expiration time ratio are extracted from the respiration signal. Due to the fast temporal changes of these features, the mean and the standard deviation (SD) of these signals are studied in 2-min time intervals.

2.2.1 Respiration rate

Human respiration rate varies in different physiological and mental conditions. Because of the non-stationary nature of respiration signal, time-frequency analysis can be used to analyze it. A wavelet synchrosqueezed transform is used to extract the instantaneous frequency of the respiration signal. The synchrosqueezed index of a signal can be obtained as follows [13]:

$$T_s(\omega_l, b) = (\Delta\omega)^{-1} \sum_{a_k:|\omega_s(a,b)|\le\Delta\omega/2} W_s(a_k, b) a_k^{-3/2} (\Delta a)_k. \tag{7}$$

where W_s is the wavelet transform of signal. The frequency variable ω and the scale variable of the transform a are both binned and can be computed only on discrete values of a_k. The bin sizes are $a_k - a_{k-1} = (\Delta a)_k$ and $\omega_l - \omega_{l-1} = \Delta\omega$. $T_s(\omega_l, b)$ is determined only at the center of the successive bins $\left[\omega_l - \frac{1}{2}\Delta\omega, \omega_l + \frac{1}{2}\Delta\omega\right]$.

Figure 5 shows the respiration signal and the derived instantaneous breath rate.

As shown in Fig. 5, the instantaneous respiration rate has variations due to the unsteady nature of the human respiration system and the driver's movements. Therefore, it is necessary to take the mean and the SD of the respiration rate in constant time intervals, e.g. 2-min epochs.

2.2.2 Inspiration-to-expiration ratio

The inspiration-to-expiration (I/E) ratio can be extracted by measuring the respiration signal peak and valley durations. This can be achieved by applying a traditional peak and valley

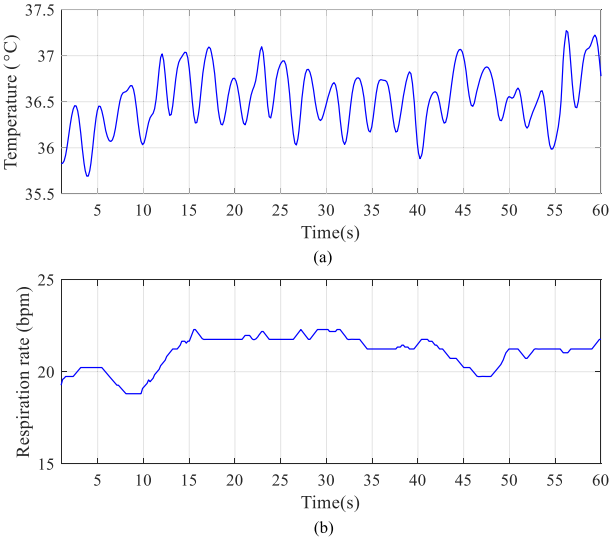

Fig. 5 (a) Respiration signal; (b) the extracted instantaneous respiration rate

detection algorithm. Figure 6 shows the extracted I/E ratio of the respiration signal derived from thermal imaging analysis.

As shown in Fig. 6, the I/E ratio has fluctuations similar to the respiration rate. Thus, it is necessary to take the mean and the SD of the I/E in constant time intervals, e.g. 2-min epochs.

2.2.3 Validation of feature extraction method

The method for obtaining the respiration rate and the I/E ratio was validated by two trained human observers. Seven healthy subjects participated in a 5-min test. The two features – the reference respiration rate and the I/E ratio – were measured at five 1-min epochs by two trained human observers. The Bland-Altman plot and the linear correlation analysis were used to evaluate the accuracy of the method. Fig. 7 and Fig. 8 show the correlation analysis and the Bland-Altman plot of the reference breathing rate (BR_{ref}) and the reference inspiration-to-expiration time ratio (I/E_{ref}) with the thermal imaging breathing rate (BR_{ti}) and the I/E ratio (I/E_{ti}).

As shown in Fig. 7(a) and Fig .8(a), both the respiration rate and the inspiration-to-expiration time ratio have a strong correlation with their reference measurement methods. All scatter points are in the 95% of confidence intervals and the regression line is close to the line of perfect match.

The Bland-Altman plots of our methods and their reference measurement methods are shown in Fig. 7(b) and Fig. 8(b). As shown in Fig. 7(b), there is a mean difference of 0.12 bpm between the proposed method and the reference breath rate, and the limits of agreement are 1.3 and − 1 bpm. All data points are within the 95% of agreement. As shown in Fig. 8(b), there is a mean difference of 0.01 between the proposed method and the reference breath rate, and the limits of agreement are 0.12 and − 0.14. Also, all data points are within the 95% of agreement.

2.3 Participants

A total number of 30 male subjects participated in the tests. The subjects signed consent forms to fully observe the experimental protocol. The study protocol was approved by the research

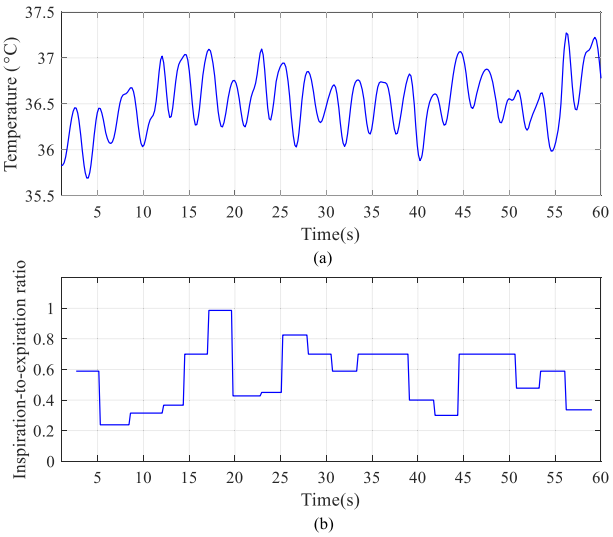

Fig. 6 (a) Respiration signal; (b) the extracted inspiration-to-expiration ratio

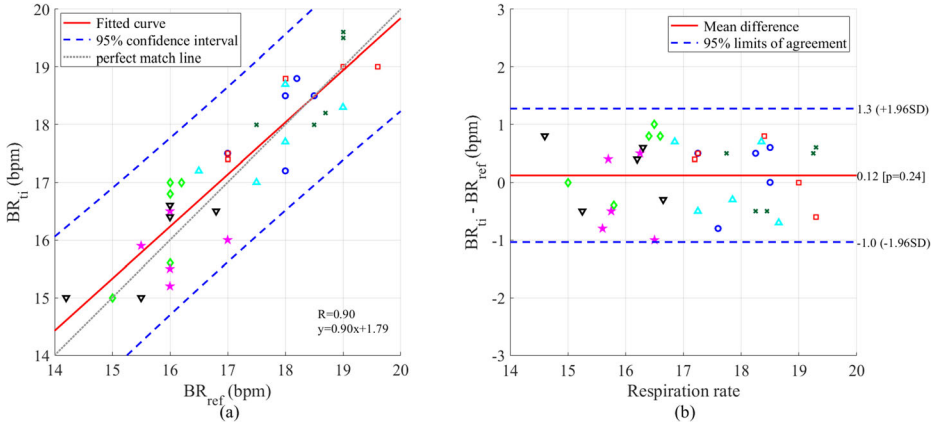

Fig. 7 (a). Correlation analysis and (b) the Bland-Altman plot for the reference breathing rate (BR_{ref}) and the breathing rate extracted from thermal imaging (BR_{ti}). Each different marker represents one subject.

ethics committee of K.N. Toosi University of Technology Research Affairs and Industrial Relations Office (RAIRO) in accordance with Declaration of Helsinki. The participants aged between 20 and 32 with the mean and SD of 26 and 2.6 years, respectively. All subjects were screened to have a regular sleep pattern with no sleep disorders. All participants were asked to undergo sleep deprivation since two days before the test; they were allowed to sleep only for 4 h at each two previous nights. The subjects were asked neither to use any caffeinated drinks nor to smoke cigarettes for a week before the test. None of the subjects was addicted to alcohol or drugs. All subjects had driving licenses with at least two years of driving experience. The tests were conducted between 11 pm to 6 am in a dark and quiet room with controlled temperature and humidity. The tests took from 20 min to 2 h. Whenever a subject crashed the car 3 times or did not fall asleep within 2 h of driving, the test was terminated. The subjects test-drove in the driving simulator for twenty minutes before the beginning of the test in order to get familiar with the car and have relaxation.

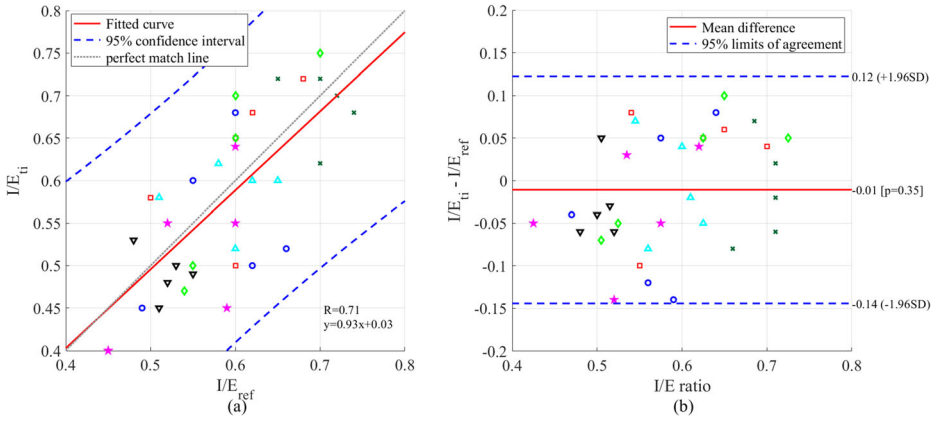

Fig. 8 (a) Correlation analysis and (b) the Bland-Altman plot for the reference inspiration-to-expiration ratio (I/E_{ref}) and inspiration-to-expiration ratio extracted from thermal imaging (I/E_{ti}). Each different marker represents one subject

2.4 Driving simulator

There are several advantages in conducting the tests in the simulator. Drowsy driving experiments in the real world are prone to fatal accidents and may be disturbed by the presence of uncontrolled inputs. Driving simulator provides a controlled driving environment and makes it possible to test the same scenario repeatedly by avoiding unexpected events without any risk to the drowsy driver. Recent studies showed that the signs of sleepiness and the development of sleepiness over time are generally similar in the simulator and the real road, though the drowsiness level is higher in the simulator [20]. Similar to our work, many researchers conducted their experiments in a simulated driving environment in other driver drowsiness studies [14, 25, 31, 37, 38, 58, 59].

A driving simulator was used to study drivers during drowsiness. The driving simulator used to conduct the drowsiness tests is shown in Fig. 9. The interior of this fixed-platform simulator is exactly the same as that of a real sedan. The dynamic model of the car has 14 degrees of freedom solved in real time. The lateral force from the road is applied to the steering wheel by an AC 1 kW servomotor.

2.5 Driving scenario

The driving path was a 67-km closed-loop three-lane highway with soft turns and no traffic. The schematic of the designed road is shown in Fig. 10. The subjects were asked to drive in the middle lane with a speed between 70 km/h to 90 km/h.

2.6 Data record

The driver's thermal image was captured with a thermal camera. The thermal camera captures video at the rate of 7.5 frames per second. The camera uses uncooled vox micro-bolometer detector with NETD of 50 m-kelvins and resolution of 640*512 pixels. Room temperature and humidity can affect thermal camera performance and

Fig. 9 The sedan driving simulator used for the tests. It dynamic model has 14 degrees of freedom. It uses an ac servomotor to apply torque to the steering wheel proportional to the tire lateral force

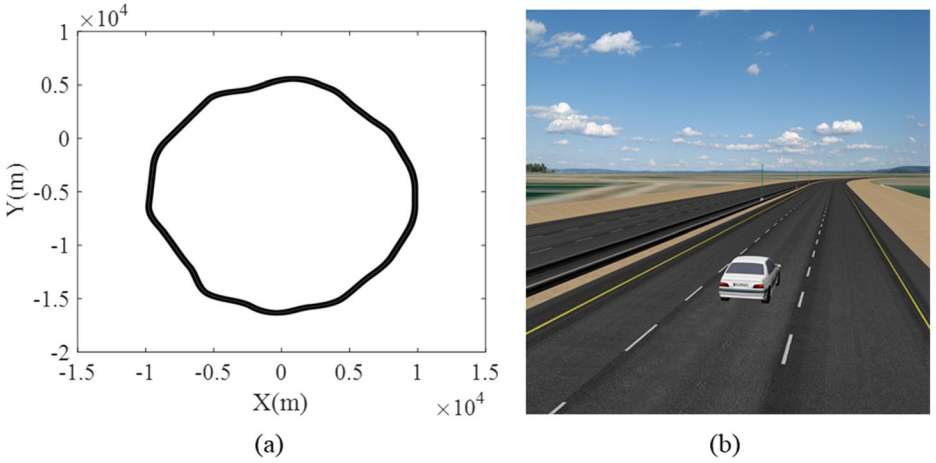

Fig. 10 (a) Driving path without graphical rendering; (b) part of driving scene with graphical rendering

the outputs. Thus, it is important to keep environmental variables stationary during the tests. In this paper, the tests were conducted in a controlled closed room to decrease measurement errors. The mean and SD of temperature and humidity were approximately 23.31 °C (0.16 °C) and 45.61% (0.15%) during the tests.

Additionally, an infrared camera captured the driver's face and body to monitor driver behavior from wakefulness to drowsiness. Figure 11 shows the location of the data recording devices in the driving simulator during the tests.

As shown in Fig. 11, thermal camera is placed in front of the driver on the dashboard. Camera angle is adjusted in a way that the driver's face is fully visible in the thermal camera field of view.

2.7 Drowsiness scale

There are several methods to evaluate the level of driver drowsiness without using physiological signals [1, 28, 61]. One method is to evaluate driver drowsiness by the Karolinska Sleep Scale (KSS) [1]. The KSS is a self-explanatory method in which the driver expresses her/his drowsiness level from 1 to 9 every 5 min. The biggest drawback of this method is its self-explanatory nature. Self-introspections alert the driver and reduce her/his drowsiness level [49]. Also, as the driver's level of drowsiness increases, the accuracy of the driver's cognitive judgment decreases which makes this scale less reliable.

The Observer Rating of Drowsiness (ORD) is an efficient and non-intrusive method to evaluate the level of driver drowsiness based on several human observers' judgments [61]. The subjects' drowsiness levels are evaluated by 3 dedicated and expert observers offline. Instead of the primitive version of the ORD method, a developed and evaluated version of the ORD method was used in this paper which described the drowsiness rating comprehensively [61]. The method used in [61] shows high inter-rater reliability. The observers track each driver's facial and behavioral signs as the level of drowsiness changes. They designate the levels of driver drowsiness by a number from 1 to 5: not drowsy, slightly drowsy, moderately drowsy, very drowsy, and extremely drowsy. The overall drowsiness score is obtained by taking the average scores of the three observers.

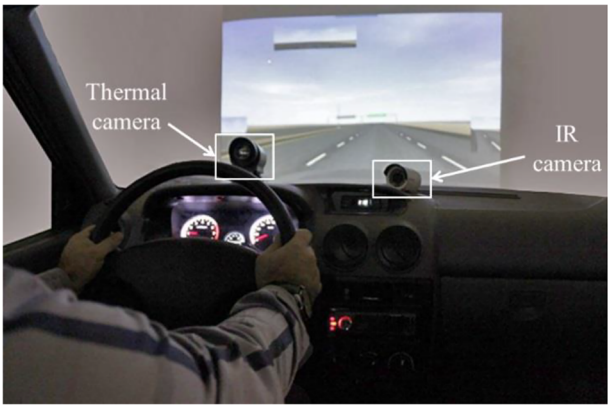

Fig. 11 Data recording tools location in the driving simulator

2.8 Data classification

Support Vector Machine: Support vector machine is a traditional supervised learning algorithm, which is used for both data classification and pattern recognition purposes. The goal of SVM along with all other data classification tools is to find a decision surface to split the dataset into two parts. SVM finds a unique decision surface with maximum margin from the dataset. The data points at each side of the decision surface are considered as members of a different class. The SVM was introduced by [10] and has been in development ever since.

In this paper, the SVM model inputs are the mean and standard deviation of the respiration rate and the I/E ratio and the output is the awake/drowsy state of the driver.

K-nearest Neighbors: The K-nearest Neighbors (KNN) method is an instance-based learning method. This method is based on the principle that the instances within a dataset will generally exist in close proximity to the other instances that have similar properties [33]. The KNN method locates the k nearest instances to the query instance and determines its class by identifying the single most frequent class label [33]. Several metrics can be used in the KNN method. In this paper, the Euclidean distance is used as the distance metric.

3 Results

After receiving the respiration signal from the thermal imaging, some features of the respiration system such as the respiration rate and the I/E ratio are extracted. The mean and SD of respiration rate and I/E ratio are analyzed in 2-min time intervals.

An ORD score of 3 or higher is considered as hazardous and may potentially result in a driving accident. Thus, the ORD score of 3 is considered as the binary threshold of wakefulness and drowsiness in this paper. The ORD<3 is considered as wakeful and the ORD> = 3 is considered as drowsy in the present study. In Fig. 12, the mean respiration rate and the mean I/E of all subjects during wakefulness (ORD = 1), moderate drowsiness (ORD = 3), and extreme drowsiness (ORD = 5) are shown.

As shown in Fig. 12 (a), the mean respiration rate of subjects decreases as drowsiness increases. At ORD = 3, a significant reduction in the respiration rate happens, which can be

used as a leading indicator for detection of drowsiness. In Fig. 12 (b), the mean I/E ratio generally rises as drowsiness increases. For twelve subjects, the I/E ratio increases only slightly from moderate (ORD = 3) to extreme (ORD = 5) drowsiness. Even for these subjects, the I/E ratio at ORD = 5 is more than that at ORD = 1. For subject #6, the I/E ratio at the extreme drowsiness state was lower than that at the moderate drowsiness state, yet both ratios are more than the ratio at the wakefulness state. For subject #7, the I/E ratio at both moderate and extreme drowsiness state are lower than that at the wakefulness state, which reduces the accuracy of the drowsiness classification. For subject #20, the I/E ratio at the wakefulness and moderate drowsiness states are close, yet the I/E ratio at the extreme drowsiness state is still higher than those at the other two states. For subject #15, the I/E ratio at the moderate state is lower than that at the wakefulness state, yet the I/E ratio at the extreme drowsiness state is still higher than those at the other two states.

Figure 13 shows the respiration rate and the I/E ratio along with the ORD rating of the subject whose respiration signal was previously shown in Fig. 3. The large peaks in respiration rate and I/E ratio are due to the movements of the driver's head and also the instant changes of the respiration rate or the I/E ratio of the driver. As shown in Fig. 13, the mean respiration rate drops as the driver's ORD rating increases and the SD of the respiration rate increases. Also, the mean and the SD of I/E ratio increases.

The normal respiration rate and the I/E ratio of subjects are different from each other because of individual differences in physiological and mental conditions. Thus, using respiration rate changes from wakefulness (ORD = 1) to drowsiness (ORD>= 3) can lead to more precise drowsiness detection with classifiers. Figure 14 shows changes in the mean respiration rate and the mean I/E ratio in wakefulness and drowsiness for all subjects.

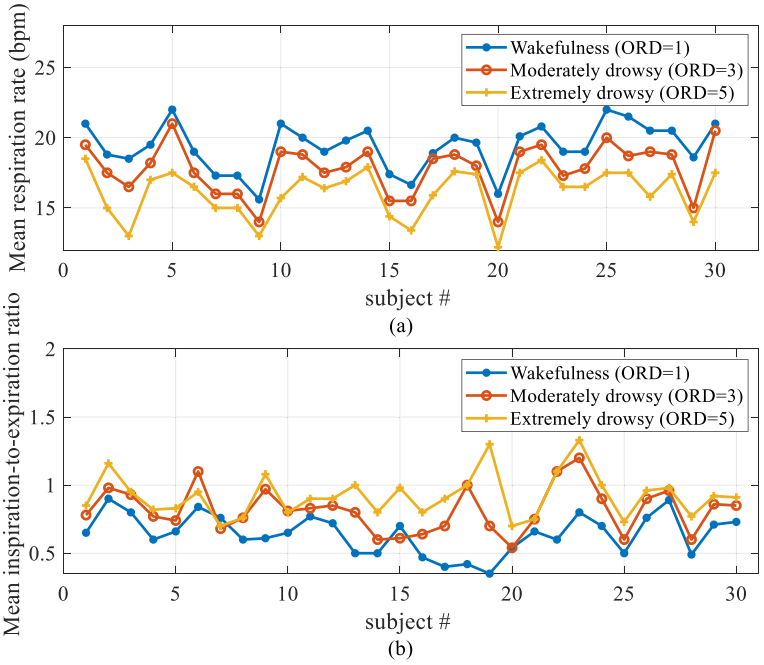

Fig. 12 (a) Mean respiration rate; (b) mean I/E for all subjects (wakefulness (ORD = 1), moderate drowsiness (ORD = 3), and extreme drowsiness (ORD = 5))

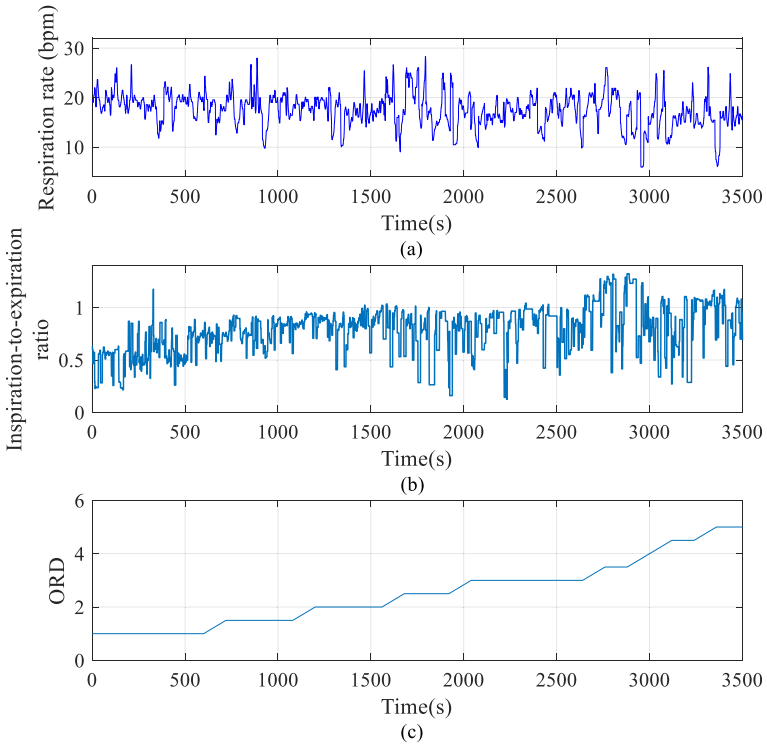

Fig. 13 (a) Respiration rate; (b) I/E ratio; and (c) ORD rating of subject # 27 during a drowsiness test

As shown in Fig. 14 (a), the mean respiration rates of drivers for the three levels wakefulness, moderate drowsiness, and extreme drowsiness are 19.6, 18.1, 16.5 bpm, respectively. The respiration rate decreases by 1.5 bpm from wakefulness (ORD = 1) to moderate drowsiness (ORD = 3). Similarly, the mean respiration rate decreases by 3.1 bpm from wakefulness (ORD = 1) to extreme drowsiness (ORD = 5). As shown in Fig. 14 (b), the I/E ratios of drivers for the three levels wakefulness, moderate drowsiness, and extreme drowsiness are 0.65, 0.80, 0.90, respectively. The I/E ratio increases by 0.15 from wakefulness (ORD = 1) to moderate drowsiness (ORD = 3). Similarly, the I/E ratio increases by 0.25 from wakefulness (ORD = 1) to extreme drowsiness (ORD = 5). The algorithm is capable of detecting moderate drowsiness. This early detection provides a margin of safety long before the driver becomes very drowsy (ORD = 4) or extremely drowsy (ORD = 5).

The evaluation of the SVM and the KNN classifiers was performed using the leave-one-out method. In order to do so, one data point was chosen as the test data; then, the training was performed using the rest of the data points. This procedure was repeated until all data points had been used as the test data once. The average accuracy, sensitivity, specificity, and precision of the trained classifiers have been calculated. The results for different classifiers using different set of features are shown in Table. 1.

Using this method, drowsiness can be detected with high accuracy and sensitivity. The best performance was achieved by the fusion of all features using the SVM classifier with the accuracy of 90%, sensitivity of 92%, specificity of 85%, and precision of 91%.

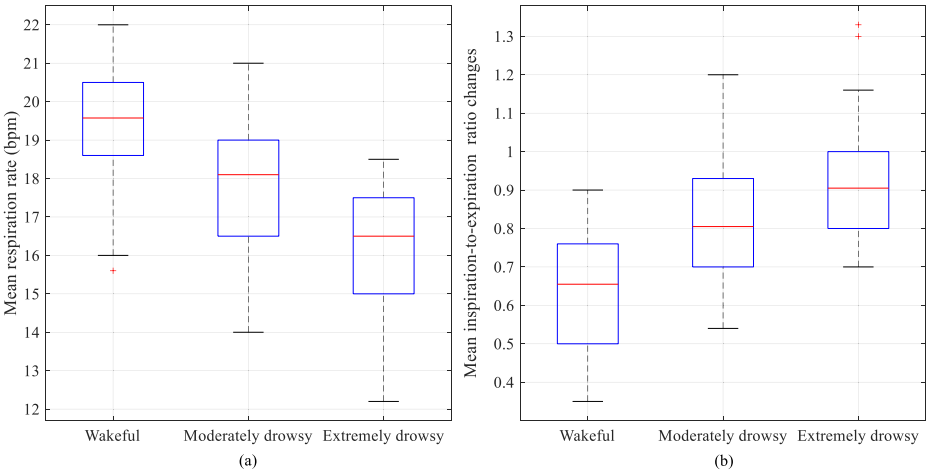

Fig. 14 (a) Mean respiration rate; and (b) Mean I/E ratio at three levels: wakefulness, moderate drowsiness, and extreme drowsiness for all 30 subjects

4 Discussion

Thermal imaging is a reliable method to monitor driver's respiration pattern, but it has its own limitations. Like every system that uses visual information, the system might locate a false region instead of the correct respiration region. Since our method uses the first 5 s of the thermal video to detect the respiration region, it is important that the driver exhibit only small movements in these initial 5 s. Situations where the nose region is covered by the driver's hand or the driver's head is turned in the first 5 s, can lead to false region localization. An initial audio warning can ask the driver to stay rather calm in the first 5 s. After the first 5 s, common driver movements do not affect the region tracking performance since the visual characteristics of the respiration region do not change. If the calculated respiration rate is not within the range of the human breathing rate, the tracker decides that the respiration region is lost. In this situation, the localization procedure is reinitiated automatically. One can use the deep learning methods to localize and track the respiration region to overcome these limitations.

Table. 1 Results of drowsiness detection system based on respiration rate (RR) and inspiration-to-expiration ratio (I/E) features

Feature	classifiers	Accuracy	Sensitivity	Specificity	Precision
Mean RR	KNN	0.81	0.82	0.80	0.86
	SVM	0.83	0.90	0.82	0.83
SD RR	KNN	0.66	0.65	0.66	0.75
	SVM	0.75	0.75	0.74	0.82
Mean I/E	KNN	0.75	0.73	0.77	0.83
	SVM	0.66	0.72	0.59	0.73
SD I/E	KNN	0.63	0.78	0.38	0.66
	SVM	0.62	0.93	0.30	0.62
Fusion of all features	KNN	0.83	0.82	0.85	0.90
	SVM	0.90	0.92	0.85	0.91

Table. 2 Comparison the accuracy of the proposed method with other respiration-based drowsiness detection studies

Study	Method	Variable(s)	Performance
Rodríguez-Ibáñez et al., 2011 [46]	Deriving a new index based on characteristics of the respiratory signal relative to the awake state	Respiratory rate variability	Sensitivity =83% Specificity = 95%
Igasaki et al., 2015 [29]	Logistic regression analysis on heart rate variability and breathing rate variability	Mean, standard deviation, and the root mean square of differences of breath rate variability and heart rate variability	Accuracy = 81%
Igasaki et al., 2016 [30]	Use of SVM for data classification	Parameters of the respiration rate	Accuracy = 89%
Lee et al., 2014 [35]	A mutual information technique to select most descriptive features for SVM classification	Combined usage of EEG features and regularity of respiration	Accuracy = 98%
Tatneo et al., 2018 [56]	Extracting respiration from ECG signals	Respiration rate	Accuracy = 64%
Guede-fernandez et al. 2019 [26]	Thoracic effort	Respiratory rate variability	Sensitivity = 93% Specificity = 96%
This paper	Using thermal imaging to extract respiration signal and using SVM for classification	Mean and standard deviation of respiration rate and inspiration-to-expiration ratio	Accuracy = 90% Sensitivity = 93% Specificity = 85%

The proposed method is robust against some unusual facial patterns, but vulnerable against some disturbances. The method is not affected by the eyeglasses, beard or facial scars because of the spatio-temporal nature of the algorithm. The method does not work well if the facial thermal pattern is altered by disturbances due to hot or cold air blowing from the air conditioner or the window. One may compensate for the effects of these disturbances by a reinforcement learning algorithm.

As shown in Fig. 1(b), the eye region can be detected and tracked using thermal imaging. Blink-related features for drowsiness detection have been used by many researchers [11, 21, 44, 51] in the visible light imaging. Blink-related features can improve the drowsiness detection in thermal imaging as well.

The high sensitivity of the thermal cameras makes them suitable for extracting features not easily accessible from regular visible light imaging. In facial thermal images, the location of the temporal artery can be obtained. Some researches focused on localizing this artery and monitored its thermal variations [8, 24, 55]. Based on a study in [63], the hidden variations of the sequential images can be visualized through video magnification methods to detect the pulse rate. Having localized the temporal artery and used the video magnification method, we can extract the pulse rate of the drowsy driver from the thermal images.

The number of studies that used respiration parameters as indicators of drowsiness is relatively small because of the intrusive nature of the conventional respiration measurement devices. Some studies that used respiration to detect drowsiness are listed in Table. 2. This comparison shows that the proposed method in this paper shows a high accuracy and sensitivity despite not using other physiological signals.

5 Conclusion

In this paper, a new drowsiness detection system was introduced based on analyzing driver respiration features using thermal imaging. It was contact-free, non-intrusive, and robust against driver's movement. Some features of the respiration system such as the respiration rate and the I/E ratio were extracted from the respiration signal. The mean and the standard deviation of the extracted features were analyzed in 2-min time intervals. The SVM and the KNN classifiers were used to classify drivers as awake or drowsy. Based on the data obtained from 30 participants, the SVM classifier resulted in the best performance in detecting drowsiness using the fusion of all respiration features with the accuracy of 90%, sensitivity of 92%, specificity of 85%, and precision of 91%.

To have a robust drowsiness detection system, a multimodal system using several sensors is preferred. Because of driver's head and body movements, the respiration region may be occluded or go out of the thermal camera viewing window. Sensor fusion can overcome the shortcomings of signal loss from certain sensors. For example, to have a robust respiration measurement system, one may choose to have a belt sensor along with the thermal camera.

In this paper, all subjects were normal people with no sleep disorder. People with narcolepsy and/or sleep apnea are at a higher risk during driving. Also, people with high body mass index have some breathing issues and are usually involved in crashes caused by drowsiness. Analysis of such cases is suggested for future studies. The effects of breathing diseases on the performance of the proposed drowsiness detection method need further investigations.

Acknowledgements This paper is based upon a work supported by the Cognitive Science and Technology Council (CSTC) under Grant No. 1307.

References

1. Åkerstedt T, Gillberg M (1990) Subjective and objective sleepiness in the active individual. Int J Neurosci 52:29–37. https://doi.org/10.3109/00207459008994241
2. Alkali AH, Saatchi R, Elphick H, Burke D (2013) Facial tracking in thermal images for real-time noncontact respiration rate monitoring. In: 2013 European Modelling symposium. Pp 265–270
3. Arefnezhad S, Samiee S, Eichberger A, Nahvi A (2019) Driver drowsiness detection based on steering wheel data applying adaptive Neuro-fuzzy feature selection. Sensors 19:943–957. https://doi.org/10.3390/s19040943
4. Balandong RP, Ahmad RF, Saeed MA (2018) A review on EEG-based automatic sleepiness detection systems for driver. IEEE Access 6:22908–22919. https://doi.org/10.1109/ACCESS.2018.2811723
5. Bartula M, Tigges T, Muehlsteff J (2013) Camera-based system for contactless monitoring of respiration. In: Annual International Conference of the IEEE Engineering in Medicine and Biology Society, pp 2672–2675
6. Bernacchia N, Scalise L, Casacanditella L et al (2014) Non contact measurement of heart and respiration rates based on Kinect™. In: IEEE International Symposium on Medical Measurements and Applications, pp 1–5
7. Chauvin R, Hamel M, Briere S et al (2016) Contact-free respiration rate monitoring using a pan-tilt thermal camera for stationary bike Telerehabilitation sessions. IEEE Syst J 10:1046–1055. https://doi.org/10.1109/JSYST.2014.2336372
8. Chekmenev SY, Farag AA, Miller WM, Essock EA (2009) Multiresolution approach for noncontact measurements of arterial pulse using thermal imaging. In: Augmented vision perception in infrared. Springer, Berlin, pp 87–112
9. Chowdhury A, Shankaran R, Kavakli M, Haque M (2018) Sensor applications and physiological features in drivers ' drowsiness detection : a review. IEEE Sensors J 18:3055–3067. https://doi.org/10.1109/JSEN.2018.2807245
10. Cortes C, Vapnik V (1995) Support-vector networks. Mach Learn 20:273–297. https://doi.org/10.1023/A:1022627411411
11. Danisman T, Bilasco IM, Djeraba C, Ihaddadene N (2010) Drowsy driver detection system using eye blink patterns. In: International Conference on Machine and Web Intelligence, pp 230–233
12. Dasgupta A, George A, Happy SL, Routray A, Shanker T (2013) An on-board vision based system for drowsiness detection in automotive drivers. Int J Adv Eng Sci Appl Math 5:94–103. https://doi.org/10.1007/s12572-013-0086-2
13. Daubechies I, Lu J, Wu HT (2011) Synchrosqueezed wavelet transforms: an empirical mode decomposition-like tool. Appl Comput Harmon Anal 30:243–261. https://doi.org/10.1016/j.acha.2010.08.002
14. De Naurois C, Bourdin C, Bougard C, Vercher J (2018) Adapting artificial neural networks to a specific driver enhances detection and prediction of drowsiness. Accid Anal Prev 121:118–128. https://doi.org/10.1016/j.aap.2018.08.017
15. Dhupati LS, Kar S, Rajaguru A, Routray A (2010) A novel drowsiness detection scheme based on speech analysis with validation using simultaneous EEG recordings. In: 2010 IEEE international conference on automation science and engineering. Pp 917–921
16. Douglas NJ, White DP, Pickett CK, Weil JV, Zwillich CW (1982) Respiration during sleep in normal man. Thorax 37:840–844
17. Fei J, Pavlidis I (2010) Thermistor at a distance: unobtrusive measurement of breathing. IEEE Trans Biomed Eng 57:988–998. https://doi.org/10.1109/TBME.2009.2032415
18. Fei J, Pavlidis I, Murthy J (2009) Thermal vision for sleep apnea monitoring. In: International Conference on Medical Image Computing and Computer-Assisted Intervention, pp 1084–1091
19. Flores MJ, Armingol JM, de la Escalera A (2011) Driver drowsiness detection system under infrared illumination for an intelligent vehicle. IET Intell Transp Syst 5:241–251. https://doi.org/10.1049/iet-its.2009.0090
20. Fors C, Ahlstrom C, Anund A, Fors C (2018) A comparison of driver sleepiness in the simulator and on the real road the real road. J Transp Saf Secur 10:72–87. https://doi.org/10.1080/19439962.2016.1228092
21. Friedrichs F, Yang B (2010) Camera-based drowsiness reference for driver state classification under real driving conditions. In: IEEE Intelligent Vehicles Symposium, pp 101–106

22. Gade R, Moeslund TB (2014) Thermal cameras and applications: a survey. Mach Vis Appl 25:245–262. https://doi.org/10.1007/s00138-013-0570-5
23. Garbey M, Sun N, Merla A, Pavlidis I (2007) Contact-free measurement of cardiac pulse based on the analysis of thermal imagery. IEEE Trans Biomed Eng 54:1418–1426
24. Gault TR, Blumenthal N, Farag AA, Starr T (2010) Extraction of the Superficial Facial Vasculature , Vital Signs Waveforms and Rates Using Thermal Imaging. In: IEEE Computer Society Conference on Computer Vision and Pattern Recognition-Workshops, pp 1–8
25. González-Ortega D, Díaz-Pernas FJ, Martínez-Zarzuela M, Antón-Rodríguez M (2019) A physiological sensor-based android application synchronized with a driving simulator for driver monitoring. Sensors 19: 399. https://doi.org/10.3390/s19020399
26. Guede-fernández F, Fernández-chimeno M, Ramos-Castro J, Garcia-Gonzalez MA (2019) Driver drowsiness detection based on respiratory signal analysis. IEEE Access 7:81826–81838. https://doi.org/10.1109/ACCESS.2019.2924481
27. Harris C, Stephens M (1988) A combined corner and edge detector. Alvey vision conference, In, pp 147–151
28. Hoddes E, Zarcone V, Smythe H, Phillips R, Dement WC (1973) Quantification of sleepiness: a new approach. Psychophysiology 10:431–436
29. Igasaki T, Nagasawa K, Murayama N, Hu Z (2015) Drowsiness estimation under driving environment by heart rate variability and / or breathing rate variability with logistic regression analysis. In: 8th international conference on BioMedical engineering and informatics. Pp 189–193
30. Igasaki T, Nagasawa K, Akbar IA, Kubo N (2016) Sleepiness classification by thoracic respiration using support vector machine. In: The 2016 biomedical engineering international conference, pp 1–5
31. Kartsch VJ, Benatti S, Schiavone PD et al (2018) A sensor fusion approach for drowsiness detection in wearable ultra-low-power systems. Inf Fusion 43:66–76. https://doi.org/10.1016/j.inffus.2017.11.005
32. Kiashari SEH, Nahvi A, Homayounfard A, Bakhoda H (2018) Monitoring the variation in driver respiration rate from wakefulness to drowsiness : a non-intrusive method for drowsiness detection using thermal imaging. J Sleep Sci 3:1–9 Retrieved from http://jss.tums.ac.ir/index.php/jss/article/view/110
33. Kotsiantis SB (2007) Supervised machine learning: a review of classification techniques. Informatica 31: 249–268. https://doi.org/10.1115/1.1559160
34. Langroodi AK, Nahvi A (2018) Design and implementation reinforcement learning algorithm for driver drowsiness detection. SAE Int J Commer Veh 11:57–64. https://doi.org/10.4271/02-11-01-0005
35. Lee B, Lee B, Chung W (2014) Mobile healthcare for automatic driving sleep-onset detection using wavelet-based EEG and respiration signals. Sensors 14:17915–17936. https://doi.org/10.3390/s141017915
36. Mahmoodi M, Nahvi A (2019) Driver drowsiness detection based on classification of surface electromyography features in a driving simulator. Proc Inst Mech Eng Part H J Eng Med. https://doi.org/10.1177/0954411919831313
37. Mcdonald AD, Lee JD, Schwarz C, Brown TL (2018) A contextual and temporal algorithm for driver drowsiness detection. Accid Anal Prev 113:25–37. https://doi.org/10.1016/j.aap.2018.01.005
38. Meng C, Shi-wu L, Wen-cai S et al (2019) Drowsiness monitoring based on steering wheel status. Transp Res part D Transp Environ 66:95–103. https://doi.org/10.1016/j.trd.2018.07.007
39. Murthy R, Pavlidis I, Tsiamyrtzis P (2004) Touchless monitoring of breathing function. In: Proceedings of the Annual International Conference of the IEEE Engineering in Medicine and Biology Society, EMBS, pp 1196–1199
40. Murthy JN, Van Jaarsveld J, Fei J et al (2009) Thermal infrared imaging: a novel method to monitor airflow during polysomnography. Sleep 32:1521–1527
41. Patel M, Lal SKL, Kavanagh D, Rossiter P (2011) Applying neural network analysis on heart rate variability data to assess driver fatigue. Expert Syst Appl 38:7235–7242. https://doi.org/10.1016/j.eswa.2010.12.028
42. Pereira CB, Yu X, Czaplik M, Rossaint R, Blazek V, Leonhardt S (2015) Remote monitoring of breathing dynamics using infrared thermography. Biomed Opt Express 6:4378–4394. https://doi.org/10.1364/BOE.6.004378
43. Philip RC, Ram S, Gao X, Rodríguez JJ (2014) A comparison of tracking algorithm performance for objects in wide area imagery. In: Southwest Symposium on Image Analysis and Interpretation, pp 109–112
44. Rahman A, Sirshar M, Khan A (2015) Real time drowsiness detection using eye blink monitoring. In: National Software Engineering Conference, pp 1–7
45. Rezaei M, Klette R (2014) Look at the driver, look at the road: no distraction! No accident! Proc IEEE Comput Soc Conf Comput Vis Pattern Recognit:129–136. https://doi.org/10.1109/CVPR.2014.24
46. Rodríguez-Ibáñez N, García-González MA, Fernández-Chimeno M (2011) Drowsiness detection by thoracic effort signal analysis in real driving environments. In: 33rd annual international conference of the IEEE EMBS. Pp 6055–6058

47. Rodríguez-Ibáñez N, García-González MA, Fernández-Chimeno M et al (2013) Synchrosqueezing index for detecting drowsiness based on the respiratory effort signal. In: XIII Mediterranean Conference on Medical and Biological Engineering and Computing, pp 965–968
48. Rohit F, Kulathumani V, Kavi R et al (2017) Real-time drowsiness detection using wearable, lightweight brain sensing headbands. IET Intell Transp Syst 11:255–263. https://doi.org/10.1049/iet-its.2016.0183
49. Sahayadhas A, Sundaraj K, Murugappan M (2012) Detecting driver drowsiness based on sensors: a review. Sensors 12:16937–16953. https://doi.org/10.3390/s121216937
50. Samiee S, Azadi S, Kazemi R, Nahvi A, Eichberger A (2014) Data fusion to develop a driver drowsiness detection system with robustness to signal loss. Sensors 14:17832–17847. https://doi.org/10.3390/s140917832
51. Schleicher R, Galley N, Briest S, Galley L (2008) Blinks and saccades as indicators of fatigue in sleepiness warnings : looking tired ? Ergonomics 51:982–1010. https://doi.org/10.1080/00140130701817062
52. Shuyan H, Gangtie Z (2009) Driver drowsiness detection with eyelid related parameters by support vector machine. Expert Syst Appl 36:7651–7658. https://doi.org/10.1016/j.eswa.2008.09.030
53. Singh S (2015) Critical reasons for crashes investigated in the National Motor Vehicle Crash Causation Survey
54. Tarassenko L, Villarroel M, Guazzi A, Jorge J, Clifton DA, Pugh C (2014) Non-contact video-based vital sign monitoring using ambient light and auto-regressive models. Physiol Meas 35:807–831. https://doi.org/10.1088/0967-3334/35/5/807
55. Tashakori M, Nahvi A, Shahidian A, et al (2018) Estimation of Driver Drowsiness Using Blood Perfusion Analysis of Facial Thermal Images in a Driving Simulator. J Sleep Sci 3:45–52. Retrieved from http://jss.tums.ac.ir/index.php/jss/article/view/122
56. Tateno S, Guan X, Cao R, Qu Z (2018) Developement of Drowsiness Detection System Based on Respiration Changes Using Heart Rate Monitoring. In: 57th Annual Conference of the Society of Instrument and Control Engineers of Japan, pp 1664–1669
57. Trinder J, Whitworth F, Kay A, Wilkin P (1992) Respiratory instability during sleep onset. J Appl Physiol 73:2462–2469
58. Wang X, Xu C (2016) Driver drowsiness detection based on non-intrusive metrics considering individual specifics. Accid Anal Prev 95:350–357. https://doi.org/10.1016/j.aap.2015.09.002
59. Wang MS, Jeong NT, Kim KS et al (2016) Drowsy behavior detection based on driving information. Int J Automot Technol 17:165–173. https://doi.org/10.1007/s12239
60. Warwick B, Symons N, Chen X, Xiong K (2015) Detecting driver drowsiness using wireless Wearables. In: IEEE 12th international conference on Mobile ad hoc and sensor systems, pp 585–588
61. Wiegand DM, McClafferty J, McDonald SE, Hanowski RJ (2009) Development and evaluation of a naturalistic observer rating of drowsiness protocol. Virginia Tech. Virginia Tech Transportation Institute
62. Wilburta LQ, Pooler M, Tamparo CD, Dahl BM (2010) Vital signs and measurements. In: Delmar's comprehensive medical assisting: administrative and clinical competencies, 4th Editio, pp 564–598
63. Wu H, Rubinstein M, Shih E et al (2012) Eulerian video magnification for revealing subtle changes in the world. ACM Trans Graph 31:1–8
64. Xie A (2012) Effect of sleep on breathing - why recurrent apneas are only seen during sleep. J Thorac Dis 4:194–197. https://doi.org/10.3978/j.issn.2072-1439.2011.04.04
65. Zhang K, Zhang L, Yang M-H, Zhang D (2014) Fast tracking via dense Spatio-temporal context learning. In: European conference on computer vision. Springer, Cham, pp 127–141
66. Zhen Z, Tsiamyrtzis P, Pavlidis I (2008) The segmentation of the supraorbital vessels in thermal imagery. In: IEEE 5th international conference on advanced video and signal based surveillance. AVSS 2008:237–244

Serajeddin Ebrahimian Hadi Kiashari received his B.Sc. degree in Electrical Engineering from Azad University, Karaj Branch in 2014 and his Master's degree in Mechatronics Engineering from K.N. Toosi University of Technology in 2017. He is a research assistant at the Virtual Reality Laboratory at K.N. Toosi University of Technology. His research interests focus on advanced driver assistance systems (ADAS), thermal imaging, biomedical signal processing, and machine vision.

Ali Nahvi received his Ph.D. degree in mechanical engineering from the University of Utah in 2003. He is currently a faculty member and the director of Virtual Reality Laboratory at K.N. Toosi University of Technology. He received the highest award of applied research by the Ministry of Science, Research, and Technology of Iran in 2018. He is a board member of Iranian Society of Mechatronics. He also serves as a board member of technology Incubator Center at K.N. Toosi University of Technology. His research interests include virtual reality, driving simulators, and drowsiness detection.

Hamidreza Bakhoda received his M.Sc. degree in mechanical engineering from K.N. Toosi University of Technology in 2016. He is a research associate of the Virtual Reality Laboratory at K.N. Toosi University of Technology. His research interests include advanced driver assistance systems (ADAS), thermal imaging, image processing and machine learning.

Amirhossein Homayounfard received his B.Sc. degree in mechanical engineering from Sharif University of Technology in 2014 and his M.Sc. degree in mechatronics engineering from K. N. Toosi University of Technology in 2017. He is a research associate of the Virtual Reality Laboratory at K.N. Toosi University of Technology. His research interests include advanced driver assistance systems (ADAS), and audio signal processing.

Masoumeh Tashakori received her M.Sc. in mechanical engineering from K.N. Toosi University of Technology in 2018. She is a research associate of the Virtual Reality Laboratory at K.N. Toosi University of Technology. Her research interests include advanced driver assistance systems (ADAS), thermal Imaging, image processing, and biomechanics.